LAWRENCE
LIVERMORE
NATIONAL
LABORATORY

LLNL-PROC-687978

Ultrashort-pulse Laser Processing of Transparent Materials: Insight from Numerical and Semi-analytical Models

N. M. Bulgakova, V. P. Zhukov, I. Mirza, Y. P. Meshcheryakov, M. Hamar, V. Michalek, O. Haderka, L. Fekete, A. Rubenchik, M. P. Fedoruk, T. Mocek

April 6, 2016

SPIE Photonics West
San Francisco, CA, United States
February 16, 2016 through February 18, 2016

Disclaimer

Ultrashort-pulse Laser Processing of Transparent Materials: Insight from Numerical and Semi-analytical Models

Nadezhda M. Bulgakova*[a,b], Vladimir P. Zhukov[c,d], Inam Mirza[a], Yuri P. Meshcheryakov[e], Martin Hamar[f], Václav Michálek[f], Ondřej Haderka[f], Ladislav Fekete,[g] Alexander M. Rubenchik[h], Mikhail P. Fedoruk[c,i], Tomáš Mocek[a]

[a]*HiLASE Centre, Institute of Physics ASCR, Za Radnicí 828, 25241 Dolní Břežany, Czech Republic;*
[b]*Institute of Thermophysics SB RAS, 1 Lavrentyev Ave., 630090 Novosibirsk, Russia;*
[c]*Institute of Computational Technologies SB RAS, 6 Lavrentyev Ave., 630090 Novosibirsk, Russia;* [d]*Novosibirsk State Technical University, 20 Karl Marx Ave., 630073, Novosibirsk, Russia;*
[e]*Design and Technology Branch of Lavrentyev Institute of Hydrodynamics SB RAS, 29 Tereshkovoi Str., 630090 Novosibirsk, Russia;*
[f]*Joint Laboratory of Optics of Palacký University and Institute of Physics ASCR, 17. listopadu 12, 771 46 Olomouc, Czech Republic;*
[g]*Institute of Physics ASCR, Na Slovance 1999/2, 18221 Praha, Czech Republic;*
[h]*Lawrence Livermore National Laboratory, Livermore, California 94550, USA;*
[i] *Novosibirsk State University, 2 Pirogova Str., 630090 Novosibirsk, Russia*

ABSTRACT

Interaction of ultrashort laser pulses with transparent materials is a powerful technique of modification of material properties for various technological applications. The physics behind laser-induced modification phenomenon is rich and still far from complete understanding. We present an overview of our models developed to describe processes induced by ultrashort laser pulses inside and on the surface of bulk glass. The most sophisticated model consists of two parts. The first part solves Maxwell's equations supplemented by the rate and hydrodynamics equations for free electrons. The model resolves spatiotemporal dynamics of free-electron population and yields the absorbed energy map. The latter serves as an initial condition for thermoelastoplastic simulations of material redistribution. The simulations performed for a wide range of irradiation conditions have allowed to clarify timescales at which modification occurs after single laser pulses. Simulations of spectrum of laser light scattered by laser-generated plasma revealed considerable blueshifting which increases with pulse energy. To gain insight into temperature evolution of a glass material under the surface irradiation conditions, we employ a model based on the rate equation describing free electron generation coupled with the energy equations for electrons and lattice. Swift heating of electron and lattice subsystems to extremely high temperatures at fs timescale has been found at laser fluences exceeding the threshold fluence by 2-3 times that can result in efficient bremsstrahlung emission from the irradiation spot. The mechanisms of glass ablation with ultrashort laser pulses are discussed by comparing with the experimental data. Finally, a model is outlined, developed for multi-pulse irradiation regimes, which enables gaining insight into the roles of defects and heat accumulation.

Keywords: femtosecond laser irradiation, dielectrics, laser-induced modification, ablation threshold, modeling

1. INTRODUCTION

Femtosecond (fs) laser processing of transparent materials is a fast-developing technique for direct writing of two- and three-dimensional optical structures such as waveguides, Bragg gratings, rewritable optical memories, etc. (see Refs. [1-15] and references therein). The technique is based on laser-induced irreversible modification of the internal material structure (and hence the refractive index change) within the focal region of the laser beam. Fs laser writing process enables deposition of laser energy in a highly localized region whose dimensions can be comparable or even smaller than the laser wavelength.[16] To induce gentle modification of the refractive index without creation of cracks and/or voids, the applied energy of the focused beam has to be small enough and its level is strongly dependent on a number of parameters such as pulse duration and numerical aperture,[11,12,17] and even such a subtle feature of laser beam as pulse front tilt.[18,19]

*nadezhda.bulgakova@hilase.cz; phone +420-314007708; hilase.cz

Laser energy deposition and final distribution of the absorbed energy are largely governed by nonlinear processes (self-focusing, multi-photon ionization, electron avalanche, etc.). These processes lead to rapid formation of a localized free-electron population, which absorbs and scatters laser light. This makes the spatiotemporal dynamics of light absorption in transparent materials complicated. To gain insight into this phenomenon, several models have been developed. One of the most popular models is based on the paraxial approximation for the laser field (the non-linear Schrödinger equation).[20-22] This model represents an important step in understanding the phenomenon of ultrafast-laser-induced modification of optical materials' properties. However, it gives only a qualitative picture of laser energy absorption. This is conditioned by the generation of a localized dense free-electron plasma, strong gradients of electron density, and light scattering to large angles. The complete set of Maxwell's equations supplemented by hydrodynamic-type equations for free electron plasma can enable a quantitative analysis at properly chosen model parameters, thus enabling prediction of laser light absorption in strongly non-linear regimes.[17,24-28] Being supplemented by themoelastoplastic simulations, such model allows to follow material relocation in softened, highly stressed material region affected by laser radiation.[28]

Choosing the model parameters for predictiing both volumetric modification and surface ablation of materials is a complicated task due to the rich physics of the phenomenon of laser energy deposition into material and its relaxation at ultrashort laser irradiation. The most of the modeling parameters are derived from theoretical considerations of the non-linear processes and experimental measurements of ablation thresholds, reflectivity, and light transmission through the sample, including pump-probe techniques.[2,29-31] Stuart et al.[2] identified the fluence thresholds for laser-induced damage (F_{th}) of fused silica glass at 800 nm wavelength in a wide range of pulse durations by microscopy inspection of the irradiated area. They have demonstrated that, in the range of pulse duration τ_L below app. 10 ps, the threshold is almost constant with some decrease toward shorter pulses while, with increasing τ_L above 10 ps, the threshold is increasing as $\sim\tau_L^{0.5}$. Du et al.[32] measured the F_{th} value as a function of pulse duration by free electron plasma lightning upon laser excitation. They found that appearance of a luminous plasma could be a good mean to identify the damage threshold in fused silica at $\tau_L \geq 10$ ps whereas, at shorter laser pulses, the threshold for plasma lightning behaves as $\sim\tau_L^{-1}$. Thus, at τ_L ~ 100 fs, luminous plasma was only observed at fluences exceeding app. 5 times the damage threshold identified in Ref. [2]. As free electron plasma luminosity can be attributed to a high electron temperature and associated bremsstrahlung radiation, its absence at near and above ablation threshold can be considered as an indication of "cold ablation" when laser generated free electrons remain at relatively low energy while ablation proceeds through photo-induced scissoring of molecular bonds. Very clean ablation features observed by Lenzner et al.[33] at ultrashort laser pulses can be perceived to be supporting the "cold ablation" mechanism. It must be underlined that the majority of numerical simulations for fused silica irradiated by femtosecond laser pulses show a good agreement with experiments on laser-induced damage threshold.[34,35] At the same time, modeling attempts of material heating for fluences well exceeding F_{th} values, which would involve the analysis of the dynamics of electron and lattice energies, are rare and demonstrate rather contradicting results. In a number of works, simulations yield extremely high electron temperatures with reaching TPa pressures that contradicts to the "cold ablation" concept.[36] Hence, the question on "cold ablation" remains open.

The majority of models refer to single pulse irradiation of materials, both in the bulk and on the surface while applications mostly utilize multi-pulsed irradiation regimes with irradiating the same material area or with scanning irradiated samples relative the laser beam so that the irradiation areas from consecutive laser pulses overlap. Hence, the models which take into account multi-pulsed irradiation features are of great demand. Such models must be accounting for heat and defect accumulation from pulse to pulse, depending on separation time between pulses and scanning velocity. Several modeling attempts are known to gain insight into heat accumulation at high-repetition-rates.[37-40] For pump-probe irradiation regimes with short time separation between pulses, dramatic impact on laser energy absorption was shown for irradiation of fused silica, both experimentally[41] and numerically,[17] due to formation of self-trapped excitons. In this work, an attempt has been done to develop a simplified model which would take into account both heat and defect accumulation.

The paper is organized as follows. In Section 2, we present the combined model based on non-linear Maxwell's equations and the equations of thermoelastoplasticity. The model describes propagation of focused laser pulses in non-linear transparent solids and evolution of materials density in the laser-affected zone after the laser pulse termination. Specific capabilities of the model are discussed, including simulations of spectra of light scattered by laser-generated plasma. In Section 3, laser ablation of glass materials is discussed. A revised model of laser-induced surface heating of dielectrics is presented with addressing the questions on the energy of free electrons upon irradiation, rate of material heating, and ablation mechanisms. The general model findings are discussed with involving experimental data of Willow

glass ablation. In Section 4, a new semi-analytical model is proposed for multipulse irradiation regimes which accounts for defect and heat accumulation and can take into account scanning velocity of the sample relative to the laser beam.

2. OPTO-THERMOELASTOPLASTIC MODEL

2.1 Main features of the model

The details of the model are presented in Refs. [17,27,28], demonstrating how the model was developed from solving Maxwell's equations[27] to accounting exciton self-trapping and re-excitation,[17] and adding the model of thermoelastoplasticity to follow laser-induced material relocation.[28] Here only its main features are touched which are important for understanding the processes accounted for in this model. Maxwell' equations for laser beam propagation through a non-linear medium can be written in the following form:

$$\frac{1}{c}\frac{\partial \vec{D}}{\partial t} - i\frac{\omega}{c}\vec{D} = -\frac{4\pi}{c}\vec{j} + \mathrm{rot}\vec{H} - \frac{8\pi}{c}W_{\mathrm{PI}}E_g\frac{\vec{E}}{\left|E^2\right|}, \tag{1}$$

$$\vec{D} = \vec{E} + \sum_m \vec{P}_m + \frac{c}{4\pi}n^2 n_2 \left|E\right|^2 \vec{E}, \tag{2}$$

$$\frac{\partial \vec{P}_m}{\partial t} - i\omega\vec{P}_m = \vec{V}_{Pm}, \quad \frac{\partial \vec{V}_{Pm}}{\partial t} - i\omega\vec{V}_{Pm} = -\omega_m^2(\vec{P}_m - B_m\vec{E}), \tag{3}$$

$$\frac{1}{c}\frac{\partial \vec{H}}{\partial t} - i\frac{\omega}{c}\vec{H} = -\mathrm{rot}\,\vec{E}. \tag{4}$$

Here $\vec{E}$, $\vec{D}$, $\vec{H}$, ω, $\vec{j}$, and c are respectively the electric field, electric displacement field, magnetic field, laser light frequency, electric current, and speed of light; W_{PI} is the rate of photoionization determined below; E_g is the material bandgap which is dependent on the field strength. The linear part of the media polarization is modeled as a set of oscillators [27] with $\vec{P}_m$ and $\vec{V}_{Pm}$ to be the local material response and its derivative respectively (Eq. (3)). The coefficients ω_m and B_m (m = 1,2,3) provide the linear refraction index value n = 1.45 for fused silica at the wavelength λ = 800 nm. n_2 is the non-linear index of refraction. Maxwell's equations are supplemented by the hydrodynamic-type equations for the free electron plasma

$$\frac{\partial n_e}{\partial t} = W_{\mathrm{PI}} + W_\sigma - \frac{n_e}{\tau_{\mathrm{tr}}}, \tag{5}$$

$$\frac{\partial (n_e\vec{\mathrm{v}})}{\partial t} - i\omega n_e\vec{\mathrm{v}} = n_e\frac{e}{m_e}\vec{E} - n_e\vec{\mathrm{v}}\left(\frac{1}{\tau_{\mathrm{c}}} + \frac{1}{\tau_{\mathrm{tr}}}\right), \tag{6}$$

$$\vec{j} = -n_e e\vec{\mathrm{v}}. \tag{7}$$

Here e is the elementary charge; m_e is the electron mass; τ_{tr} is the characteristic time of electron trapping into excitonic states (τ_{tr} = 150 fs).[41] For simplicity, the collisional ionization rate in Eq. (5) is described via the Drude formalism.[28] The electron scattering time τ_c is also simplified to be taken equal to 1.27 fs accounting that the damping factor $\omega\tau_c$ = 3.[22] Note that Eq. (6) governs acceleration of free electrons in the laser field and the loss of their momenta. Thus, it provides information on the average energy of free electron population. Hence, the Maxwell-based approach does not require assumptions on the rate of *free electron absorption* as this process is described via coupling of the free electron current (Eqs. (6)-(7)) with Maxwell's equation (1).

The system of equations (1)–(7) is solved for fused silica irradiated by femtosecond laser pulses, using a finite-difference-overstepping numerical scheme. Here we report the examples of laser pulses of a Gaussian spatial and temporal shapes focused inside fused silica glass though the code can be applied to various beam shapes with different

polarization states, including optical vortices (to be published), as well as to other transparent solids. Description on the initial and boundary conditions can be found in Refs. [17,27,28]. The computational region (glass sample) is taken thick enough to ensure that there is no noticeable laser energy absorption both on the front and rear sample surfaces. Upon simulations, the instanteneous snapshots of the free electron density and laser intensity are recorded to gain insight into developing the free electron plasma and its influence on the laser beam propagation. The laser energy absorbed by matter locally in each grid cell (E_{abs}) is integrated over time.

When laser beam leaves the computational region, the obtained spatial map of the absorbed energy can serve as initial conditions for applying the thermoelastoplastic model.[28] The lattice temperature T after electron – lattice relaxation can be estimated as $T = T_0 + E_{abs}/c_p\rho$ where T_0 is the initial sample energy, c_p is the material heat capacity (in the general case, dependent on the temperature), and ρ is the material density. In this Section the defect formation is not considered. It is assumed that the total energy from the electronic subsystem, including the bandgap energy E_g, is finally transmitted to the lattice heating. Although free electrons are first trapped to the self-trapped exciton (STE) states, the STE population decays at sub-nanosecond time after excitation[42] and only a small fraction on the STE (~10^{-3}) transforms into the defect states such as E'-centers.[43] After obtaining an instantaneous distribution of the temperature inside laser-irradiated glass which yields also the distribution of stress in swiftly heated material volume, the 3D classical model of thermoelastoplasticity[44] is applied in order to elucidate the dynamics of elastic waves and final plastic deformations. The details of the model and modeling parameters for fused silica are described in Ref. [45].

2.2 Laser energy absorption and material density evolution

In Figure 1, the results of simulations are presented for the Gaussian laser beam of 45 fs duration focused into fused silica (pulse energy of 2 μJ, NA = 0.25, geometrical focus is at 120 μm from the sample surface). The peak absorbed energy (Fig. 1(b)) is ~1840 J/cm^3 that is smaller than that calculated for a longer beam of smaller energy (compare with the results obtained for a 1-μJ beam of 150 fs duration[28]). This behavior corresponds to the overall tendency reported in Ref. [17]: the longer the pulse duration, the more effective local absorption can be reached. However, the peak absorbed energy, being converted to the temperature map, exceeds the annealing point of fused silica. This indicates that local modification of refractive index in softened material can be expected in this case.

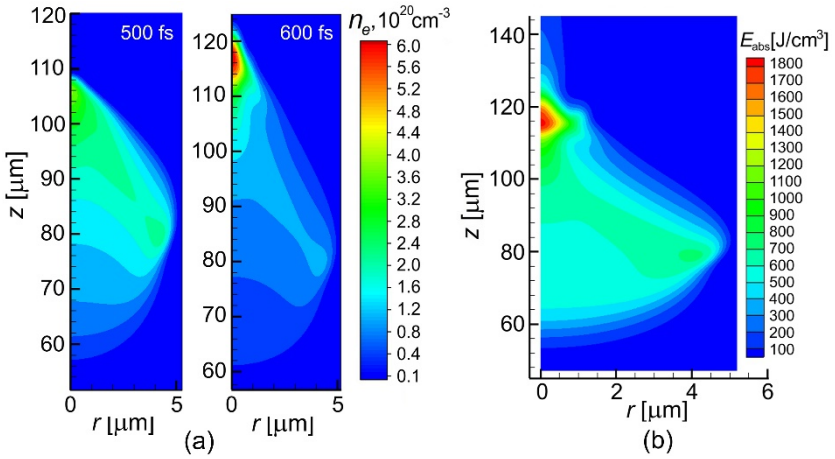

Figure 1. (a) Free electron density snapshots in fused silica glass for 2-μJ laser beam of 45 fs duration focused to the depth of 120 μm below the sample surface with NA = 0.25. (b) The distribution of the absorbed laser energy after laser beam termination.

After obtaining an instantaneous distribution of the temperature and stress in swiftly heated material volume, the dynamics of elastic waves can be elucidated with addressing final plastic deformations. Figure 2 (left) demonstrates snapshots of glass density in the laser-excited region in the regime when locally the glass is heated above the melting temperature[28] (pulse energy is 2.5 μJ with duration of 80 fs; NA = 0.32). Stress-induced density redistribution can already be noticed at timescale ~15–20 ps.[28] At early times, the hottest zone created by light absorption on the axis of the laser-excited region rapidly expands (blue spot indicating decreased density). At these time moments, a compression wave is generated at the edges of the cone-like laser-heated structure due to strong temperature gradients whose values at these sites exceed 100 K/μm. Further dynamics of material motion is rather complicated (see Ref. [28]). An intriguing dynamics of material density evolution continues up to times of order of several microseconds after which the final

modification structure is stabilized (left bottom corner in Fig. 2). For predicting the deformation structure upon stress-wave propagation in the material, we use the von Mises yield criterion. It is based on the assumption that plastic deformation of a material begins when the sum of squares of the principal components of the deviatoric stress reaches a certain critical value, namely the yield stress.[44,45] Interesting is that, in spite of a long evolution of the material with complicated density relocation dynamics, the final deformation picture imprinted in glass is very similar to that developed at times of order of several dozens of picoseconds (compare the final structure with that at t = 32 ps).[28] However, our simulations of the stress evolution show that namely at this time scale the von Mises criterion is fulfilled while already at $t \geq 100$ ps the stress levels are essentially relaxing. So, the further intricate evolution of glass density up to microsecond timescale which is observed in these simulations and also experimentally[46] is caused by elastic waves. The latter cannot cause any damage to the material matrix though the matter "breathes" acoustically up to microseconds that can be erroneously perceived as a far-reaching effect.

For the irradiation conditions shown in Fig. 2, left, simulations predict a local melting in the near-focal region with the tensile stress in this region exceeding several dozens of MPa.[28] According to the scenario, proposed by Bellouard and Hongler,[47] bubble formation may be initiated via homogeneous nucleation of the vapor phase due to large degree of expansion. As a result, the molten material occurs deeply superheated into the metastable state where the rate of homogeneous nucleation of the vapor phase grows exponentially.[47] For fused silica glass, vapor phase is formed via the following reaction: $SiO_2(l) = SiO(g) + 0.5O_2(g)$ with l and g referring to the liquid and gas phases. The scheme of bubbles coalescing into a single bubble is shown in Fig. 2 (right middle). Depending on the depth of superheating into the metastable region, single or multiple bubbles can be produced in the stretched liquid region of high temperature (1). Even if the multiple bubbles are produced, they can evolve into a single bubble if their characteristic diffusion time for coalescence is smaller than material cooling time to the temperature below the melting point and/or they continue to grow. Due to strong temperature gradients in the laser-heated region, each bubble, even being very small, has different temperatures in its different walls and tends to migrate in the direction to a hotter zone driven by the difference in surface tension (2).[48] Finally the bubbles coalesce into a single bubble (3).

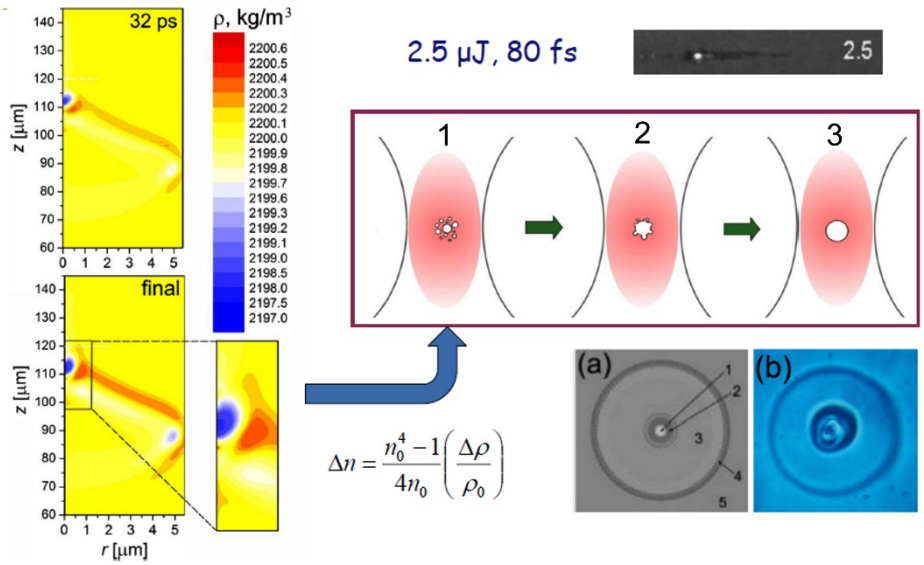

Figure 2. *Left*: Modification of fused silica density after propagation of 2.5-μm laser beam of 80-fs duration focused at the depth of 120 μm with NA = 0.32. The final density map is also shown with magnification of the region of lowest density. Note that the final density profile resembles the density structure which forms at several dozens of picoseconds. This regime corresponds to the conditions of experiments [22] when a void-like feature is observed at phase-contrast microscopy (shown on the *right top side*). *Right middle*: Illustration on how the bubble formation can develop in the laser-excited molten region inside glass (see text). *Right bottom*: (a) Integration of the final density change (shown on the left) along the laser beam propagation direction. The darker area corresponds to higher "positive" change of density and, hence, higher refractive index (see expression[49]). Two compacted ring-like regions (2 and 4) are seen, one around the expanded core (1) and another at the boundary of modification region (4) behind which virgin glass is preserved (5). In the region 3 the integral density change along the laser beam propagation direction is negative. (b) Modification structure in BK7 created by exposure with femtosecond near-IR laser pulses during 0.05 s at 1 MHz repetition rate (adopted from Ref. [50]).

The density evolution lasts in the simulations to microsecond timescale that is in line with recent observations.[46] This gives hopes that the model can also predict the geometry and the degree of final modification with reasonable precision. For direct comparison, note that, according to the Lorenz-Lorentz relation, the refractive index change Δn induced by material compaction/expansion is proportional to the density change $\Delta\rho$ (see expression in Fig. 2 with n_0 and ρ_0 to be the refractive index and the density of virgin material respectively).[49] Based on this relation, the final density change was integrated along the direction of laser beam propagation (right bottom (a)). Such modification structure is typical for fs laser exposure of glasses[50,51] and its radius depends on pulse energy, repetition rate and exposure time.[51] For small number of pulses applied to fused silica, modification diameters are comparable to that obtained in modeling, of order of 10 μm.[51]

2.3 Angle-dependent spectrum of laser beam upon electron plasma formation and scattering inside glass

If a laser pulse rapidly ionizes a medium, the refractive index of the latter is dynamically decreases, resulting in increasing speed of light in the medium and, hence, in a frequency blueshift.[52,53] The frequency shifts can be used as quantitative diagnostic means for plasma dynamics in ionizable media.[52-54] The blue shift $\delta\omega$ can be estimated by integration of the wave number variation δk, which is induced by to the creation of free electron plasma, along the laser beam pass as $\delta\omega \approx -\frac{\partial}{\partial t}\int \delta \mathrm{k} dz$. This expression can be roughly rewritten as

$$\delta\omega \sim \mathrm{k}_0 d \frac{\partial}{\partial t}\left(\frac{\omega_p^2}{2\omega^2}\frac{n_e}{n_{cr}}\right). \tag{8}$$

Here k_0 is the wave number of the incident carrier wave, d is a size of field localization (ionization region), ω_p is plasma frequency, and n_{cr} is the critical plasma density. Expression (8) shows that the blue shift grows up with the increase of the electron plasma density and the size of the ionization region. As the electron density is swiftly changing, strong broadening of the beam spectrum has to be observed.

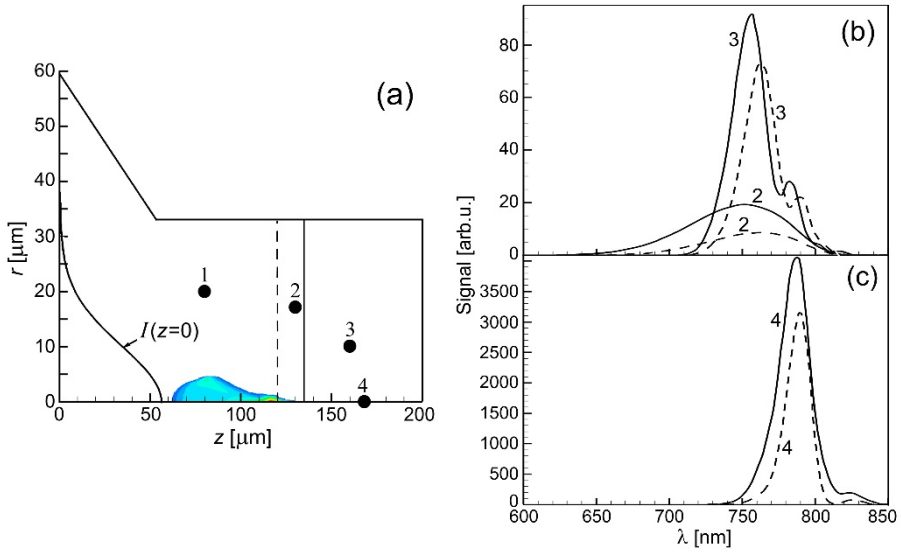

Figure 3. Illustration of laser light scattering and blue shift. (a) Absorption region (colored) and the points where laser light spectrum has been calculated. (b),(c) Spectra of transmitted and scattered light for the beam energies of 2 μJ (solid line, irradiation parameters correspond to Fig. 1) and 1μJ (dashed line; the other irradiation parameters as for 2 μJ).

In simulations, the spectrum of the electric field of the laser wave is calculated as

$$E_\omega^2 = E_{\omega r}E_{\omega r}^* + E_{\omega\varphi}E_{\omega\varphi}^* + E_{\omega z}E_{\omega z}^* \tag{9}$$

where $E_{\omega\alpha} = \int_0^\infty E_\alpha(\vec{r},t)\exp(i\omega t)dt$ (α = r, φ, z) in the points which are shown in Fig. 3(a). The irradiated parameters correspond to Fig. 1. For these conditions, the radiation scattering in the directions perpendicular to the plasma and backward to the laser is rather small but can become considerable for larger beam intensities and longer laser pulses (to be published). As the intensity of scattered light in the point 1 is ~10^8 times smaller as compared to the point 4 (light transmitted through the plasma region), we do not show the spectrum for this point. The light intensity signals in the points 2 and 3 are also weaker, but not negligible, as compared to that at the point 4. The point 3 is placed at a distance from the axis which corresponds to the edge of the light beam after its passing the focal region. In the point 2, only the scattered radiation is detected that can be registered in experiments for the sake of diagnostics of laser-induced plasma. The blue shift and spectrum broadening increase from the point 4 to point 2. We underline that the spectra have significant differences for the different pulse energies and pulse durations. Further studies of the spectral broadening and blushifting aspects are under progress, including the possible influence of blue shift on the ionization dynamics.

3. SURFACE ABLATION OF FUSED SILICA: DIFFERENCES FROM VOLUMETRIC IONIZATION DYNAMICS

In this Section we address the irradiation conditions when the laser beam is focused on the sample surface with inducing the surface damage and ablation. Large body of work has been performed by the groups over the world, both experimental and theoretical, with addressing the complicated phenomenon of optical materials damage and glass drilling and cutting (Ref. [55] and references therein). However, still this complicated phenomenon is not completely understood due to large number of linear and nonlinear processes which are interfering in space and time. One of the most important questions is the energy and density of produced electron plasmas. For the cases of volumetric modification of transparent materials, the free electron plasma regulates its parameters: as soon as the laser beam tends to collapse, swiftly generated electron population displaces the laser light from the plasma region.[17,22,27,28] This ensures, for relatively small and moderate focusing angles, the laser intensity clamping effect resulting in subcritical free electron densities with relatively low energies. By other words, the laser intensity is delocalized by free electron plasma generation, the effect that is not pronounced upon focusing on the sample surface.

The majority of numerical simulations for fused silica glass irradiated by femtosecond laser pulses are performed for the irradiation conditions nearby the ablation threshold F_{th} (the laser fluence value at which material ablation is initiated). The most of them demonstrate a good agreement with experiments on the F_{th} values[34,35] and predict the craters profiles based on a simplified ablation criterion.[56] For higher laser fluences, noticeably above F_{th}, the modeling attempts are mostly limited to the simulations of free electron density while of material heating dynamics is not usually analyzed. In a number of works, simulations yield extremely high electron temperatures with reaching TPa pressures that contradicts to the “cold ablation” concept.[36] As mentioned above, the question on “cold ablation” remains open. Here we address this contradicting question and show that the concept of “cold ablation” looks to be doubtful. We do not touch the regimes of few laser cycle pulses, when high electron current on the dielectric surface can be generated without inducing any observable damage of the material.[57] The irradiation conditions with femtosecond laser pulses which become popular for technological applications are considered below.

3.1 Revisiting the model of surface ablation of transparent dielectrics

In addressing the high-intensity irradiation of transparent materials with ultrashort laser pulses, we use the basic equations of the drift-diffusion approach which was developed to gain insight into laser-induced surface charging.[58,59] As was shown,[59] the electron photoemission process does not affect noticeably heating of the material. Hence, to simplify the task similarly to Ref. [60], photoemission and charge separation are disregarded, thus removing the necessity of consider the Poisson equation that overcomplicates simulations.

The simplified model, though allowing for simulations of the lattice heating process, consists of the rate equations for the free electrons and exciton states generation, calculation of the optical response of swiftly developing electron plasma, and the heat equations in the form of the two-temperature model (TTM). When considering TTM, we remember that the electron subsystem cannot achieve complete thermalization during a femtosecond laser pulse.[61] Hence, the electron temperature is treated as a measure of the average electron energy. The complete set of equations can be found in Refs. [58-60]. Here we underline only the differences and new features which have been introduced into the present model.

The rate equation for the evolution of laser-generated charge carriers was rewritten into two equations describing generation of both free electrons and self-trapped excitons (STE) emerging from the free electron trapping process:[22]

$$\frac{\partial n_e}{\partial t} = W_{PI} + W_{PI}^{STE} + W_{av} - \frac{n_e}{\tau_{tr}}, \tag{10}$$

$$\frac{\partial n_{STE}}{\partial t} = -W_{PI}^{STE} + \frac{n_e}{\tau_{tr}} - n_{STE}\left(\frac{1}{\tau_{rec1}} - \frac{1}{\tau_{rec2}}\right). \tag{11}$$

Here n_{STE} is the STE density; τ_{tr} is the characteristic trapping time (taken to be 150 fs)[62]; τ_{rec1} = 34 ps and τ_{rec2} = are the exciton decay time described by a bi-exponential function.[42] Trapping of the conduction electrons occurs into the deep states in the bandgap characterized by the absorption peak at 5.2 eV.[62] Hence, four-photon laser excitation of the STEs by the laser beam at 800 nm wavelength can be assumed. The photo-ionization rates for valance electrons and the electrons trapped in the STE states were written respectively in the forms[22]

$$W_{PI} = W_{PI0}\left(\left|E^2\right| / E_*^2\right)^K (n_{at} - n_e - n_{STE}) / n_{at}, \tag{12}$$

$$W_{PI}^{STE} = W_{PI0}^{STE}\left(\left|E^2\right| / E_*^2\right)^{K_{STE}} n_{STE} / n_{at}. \tag{13}$$

Here E is the electric field, n_{at} is the atomic density of the material, $E_*^2 = 8\pi I_* / nc$ is the laser intensity at which the Keldysh parameter $\gamma = 1$ ($I_* = 3.5\times10^{13}$ W/cm^2), $K = 6$ and $K_{STE} = 4$ are the orders of multiphoton ionization of valence and trapped electrons, W_{PI0} and $W_{PI0}{}^{STE}$ are the multiphoton ionization constants for valence and trapped electrons respectively ($W_{PI0} = 3.7\times10^{34}$ cm$^{-3}\cdot$s^{-1} and $W_{PI0}{}^{STE} = 2\times10^{37}$ cm$^{-3}\cdot$s^{-1}).[62,63] The avalanche ionization rate W_{av} is kept in the form as given in [19]. We assume that the electron trapping can start at the last quarter of the laser pulse when the beam intensity drops. During the laser pulse when free electrons are oscillating in the high-intensity wave field, the trapping process considered improbable.

The avalanche term is taken in the form $W_{av} = \nu_{col} n_e$ where the electron collision frequency ν_{col} is evaluated as[24]

$$\nu_{col} = \alpha_0 (n_{at} - n_e)\left[(\beta/\pi)^{0.5}(7.5\beta - 1)\exp(-\beta^{-1}) + (3.75\beta^2 - 3\beta + 1)\mathrm{erfc}(\beta^{-0.5})\right], \tag{14}$$

where $\beta = 1.5T_e/E_g$ is the normalized electron temperature; $\alpha_0 = 1.5$ fs^{-1}.

Consequently, the attenuation of the laser beam toward material depth is simulated as

$$\frac{\partial}{\partial x} I(x,t) = -6\hbar\omega W_{PI} - 4\hbar\omega W_{PI}^{STE} - a_{\mathrm{ab}}(x,t) I(x,t) \tag{15}$$

with the local absorption coefficient α_{ab} to be determined from the Drude model, together with the reflection coefficient.[58-60] In the TTM, the laser energy term accounts for all the channels of laser energy absorption and redistribution between the electrons, lattice, and STE states:

$$\frac{\partial E_f}{\partial t} = \left(6\hbar\omega - E_g\right) W_{PI} + \left(4\hbar\omega - E_g^{STE}\right) W_{PI}^{STE} - E_g Q_{\mathrm{av}} + \alpha_{\mathrm{ab}} I(x,t) - E_e \frac{n_e}{\tau_{tr}}. \tag{16}$$

As a consequence, an additional energy balance equation is solved, accounting for the energy stored in the STE states:

$$\frac{\partial E_{STE}}{\partial t} = E_e \frac{n_e}{\tau_{tr}} - \left(4\hbar\omega - E_g^{STE}\right) W_{PI}^{STE} n_{STE} - (E_g - E_g^{STE}) n_{STE}\left(\frac{1}{\tau_{rec1}} - \frac{1}{\tau_{rec2}}\right). \tag{17}$$

For the electron-lattice coupling, we take into account that this time cannot be longer than the electron trapping time and, hence, lattice heating occurs on extremely short time scale in fused silica glass. The coupling factor was taken similarly

to Ref. [35] as estimated as $\gamma_{el} = \gamma_0 n_e^{2/3}$. The system of equations (10)-(17) was solved together with the full TTM[58-60] and the Drude model for the laser beams of the Gaussian temporal shape of 130-fs duration.

3.2 Simulation results: What is the realistic electron energy?

The results of simulations for two laser fluences, 4 and 5 J/cm^2, are presented in Fig. 4. These fluences correspond to the average laser fluences 2 and 2.5 J/cm^2. In this range of fluences, the damage threshold is usually identified for the fused silica glass.[2] The final lattice temperature remains well below the annealing point at 4 J/cm^2 while, at 5 J/cm^2, it exceeds the melting point of fused silica. Hence, the model describes the damage threshold with a good accuracy. Additionally, the electron density fits quite well the measured data.[30]

While the lattice dynamics and the free electron population look to be reliable, extremely high electron energies generate some doubts. The simulated electron heating dynamics is strongly different from the volumetric focusing cases as mentioned above. Well lower electron densities generated by the laser pulse require much higher electron energies in order the energy balance could bring to the lattice heating towards the damage parameters. Furthermore, at even higher fluences, though the free electron density increases above 10^{20} cm^{-3}, the electron energy is also further increases. Thus at 8 J/cm^2, the maximum electron density is already 1.3×10^{21} cm^{-3} while the electron energy approaches 100 eV that, however, agrees with the energy of photoelectrons observed at similar laser intensities.[64] As for the lattice temperature, it experiences extremely fast heating towards a hundred thousand Kelvins. If to assume that it is feasible, two mechanisms can be speculated to be responsible for ablation, the Coulomb explosion due to highly energetic electrons escaping from the material surface layer[58,59,64] and leaving behind a high positive charge and fast atomization/dissociation of covalently bonded glass matrix. Most probably, these mechanisms can coexist at high laser intensities.

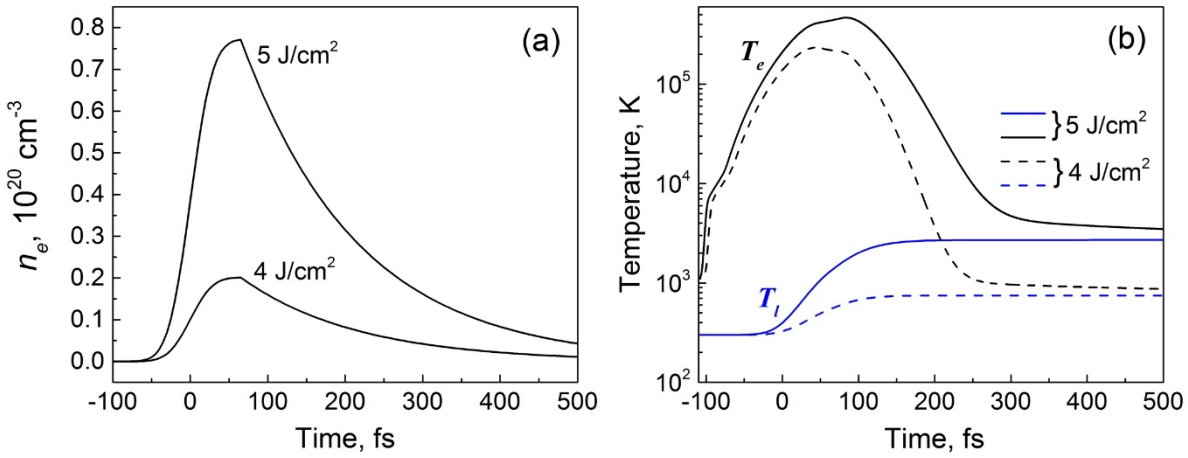

Figure 4. (a) Temporal evolution of the electron density on the sample surface for two laser fluences. The simulation fluences correspond to the average laser fluences, 2 and 2.5 J/cm^2, between which the laser-induced damage was measured in Ref. [2]. (b) The electron and lattice temperature dynamics for the same laser fluences as in (a). At 4 J/cm^2, the lattice remains relatively cold, well below the annealing point. At 5 J/cm^2, the lattice is heated above melting temperature. Hence, the model describes the damage threshold with a good accuracy.

It can be expected that extremely high energy of electrons will result in appearance of luminous plasma lightning as observed experimentally.[32] We have estimated the bremsstrahlung radiation by a classical expression[65,66]

$$Q_{brem} = 1.5\times10^{-34} n_e n_i Z^2 T_e^{0.5}. \quad (18)$$

Here the electron and ion densities ($n_i = n_e$ in the case considered here) are measured in cm^{-3} and the electron temperature is in eV. At fluences near and slightly above the ablation threshold, the bremsstrahlung intensity is negligible in agreement with experimental observation for femtosecond laser pulses.[32] Already at 8 J/cm^2, the calculated bremsstrahlung emission grows by 5 orders of magnitude and continue to grow at higher fluences. Accounting for growing the high-temperature spot on the material irradiated by the laser beam of Gaussian profile, the integral bremsstrahlung emission is growing faster with laser fluence than described by (18). Finally, starting from a definite laser intensity, plasma emission becomes detectable. These studies are now under progress. In the next Section, the measurements of plasma emission are presented linked with the profiles of the ablation craters.

3.3 Measurements of plasma emission and ablation craters

For the experimental study, we have chosen another glass material than in Ref. [2], thin samples of Corning Willow glass app. 0.1 mm thick. Prior to experiments, the samples were cleaned in an ultrasonic bath of acetone and isopropanol. Laser ablation of glass was performed using a Ti: Sapphire fs-laser (Coherent, Legend Elite fs-laser series) with wavelength of 800 nm. The maximum pulse energy was 4 mJ pulses with pulse duration of ~130 fs. The laser beam was focused on the sample surface with a 10-cm focal length plano-convex lens and the laser energy on the irradiated surface was controlled using a combination of half wave plate and polarizing beam splitter. The beam waist diameter ($1/e^2$) at focus was ~24.5 µm.

The main aim of these experiments was to measure the early-stage optical emission which was performed using a Czerny-Turner spectrometer with a focal length of 163 mm (Andor: Shamrock 163 with 1200 lines/mm grating). The emission intensity at the output of spectrometer was recorded as a function of wavelength with the help of a fast ICCD camera (Andor: iStar DH334T ICCD) with a minimum temporal resolution of 3 ns. The ICCD matrix was consisted of 1024×1024 pixels each with size of 13×13 µm. The time delay between the laser pulse and the observation gate was adjusted using built in delay generator of the ICCD. The ICCD was externally triggered by the TTL pulse from the laser system. To record the optical emission for certain laser fluence, a maximum of 50 laser shots were applied on a translating target. The velocity of the translation stage was adjusted appropriately to exclude the overlap between individual irradiation spots. Single-shot ablation craters produced on the target surface at different laser fluences were studied by scanning confocal laser microscope (Olympus LEXT: OLS 3100). The detailed crater morphology was studied by atomic force microscopy operating in tapping mode (Bruker: Dimension Icon ambient AFM in peak force modulation (an upgrade of tapping mode) with a tip diameter ≤ 10 nm). All experiments have been performed in air under atmospheric conditions.

Figure 5(a) demonstrates the white light spectra which were collected from the irradiated target and can be attributed to bremsstrahlung radiation of free electrons generated in the sample. Although intentionally we have chosen a composite glass, very different by properties from fused silica, electron plasma emission features are similar to those found for fused silica glass.[32] The ablation threshold was determined at a fluence slightly below 2.7 J/cm^2. Ablation starts steeply and already at 2.76 J/cm^2 a well-defined, 150-nm deep crater with diameter of 10 µm is observed (Fig. 5(d)). The crated is surrounded by a 80-nm high rim that indicates that this material is softer and with much lower melting point compared to fused silica where a rim is not observed under such irradiation conditions.[33] Similar to fused silica glass,[33] electron plasma emission from the sample is detected starting from ~13 J/cm^2, well above the ablation threshold. Crater diameter and depth are increasing with fluence and at 13 J/cm^2 crater is ~25-µm wide and 450-nm deep. Namely starting from fluences of ~13 J/cm^2, a “secondary crater” appears inside the ablated volume with its “secondary” rim which is well seen at higher fluences (Fig. 5(b,c)). One can speculate that most probably the secondary crater originates from superposition of two mechanisms, spallation of a wide surface layer and phase explosion/atomization in the middle part of the crater which can develop on different time scales.[67] On the other hand, bright plasma emission can also point to a Coulomb explosion from a superhot middle part of the irradiated area that is confirmed by the photoemission measurements.[64]

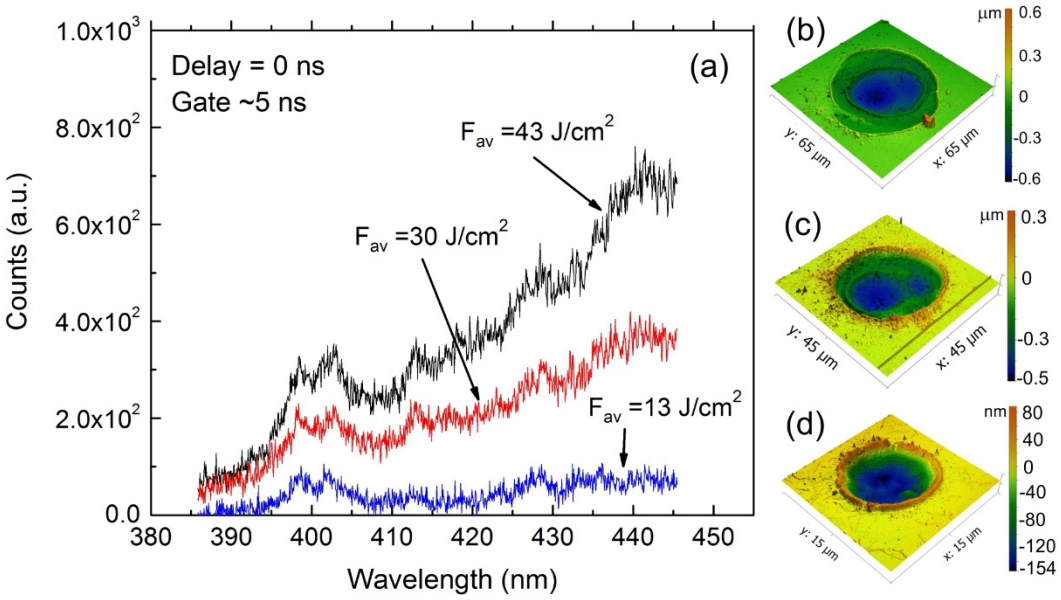

Figure 5. (a) Early stage optical emission spectra from Willow glass which can be attributed to hot electron plasma excited in the sample. Below 13 J/cm^2 emission is hardly detectable. (b)-(d) AFM profiles of single-shot ablation craters obtained with the average fluences of 59 J/cm^2 (b), 24 J/cm^2 (c), 2.76 J/cm^2 (d).

More detailed studies will be reported elsewhere (to be published). Here we add that even at higher fluences a three-rim crater is formed on the surface (Fig. 6) which, presumably, originates from several ablation mechanisms manifesting themselves at different time scales.[68] Interestingly, the crater is not strongly deepening while its diameter is considerably increasing with fluence. The fact that, the external rim is formed with the diameter exceeding more than 3 times beam diameter ($1/e^2$), can point to the effects associated with ambient gas ionization.[68,69] The aspects of ambient plasma assisted ablation call for further studies.

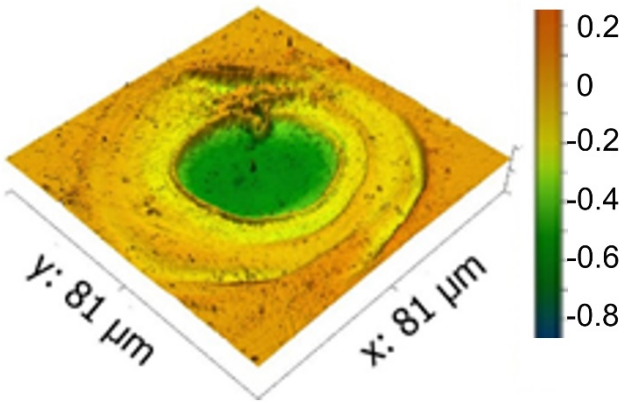

Figure 6. AFM profile of single-shot ablation craters obtained with the average fluence of 112 J/cm^2.

4. MULTIPULSE LASER PROCESSING MODEL: DEFECT ACCUMULATION

In this Section, we address the effects of heat and defect accumulation on multipulse laser processing of transparent materials that can influence the laser energy absorption both upon focusing inside the bulk and on the sample surface. Several modeling attempts exist which successfully predict the heat accumulation effects upon laser-induced modification of optical materials in multipulse irradiation regimes.[37-40,51,70] Here, based on these developments and the geometrical model of laser light absorption upon focusing ultrashort laser pulses inside glass,[71] an attempt has been made to gain also insight into consequences of the defects that are generated in materials from pulse to pulse. It can be

expected that, for multipulse irradiation regimes, defect accumulation facilitates plasma formation dynamics with pushing the electron plasma density to a higher level with each subsequent pulse and, hence, leading to a higher local absorption. However, recently we have shown that, in pump-probe experiments on fused silica excitation with ultrashort laser pulses, an exciton-mediated shielding effect is developing that results in a smaller fraction of laser beam that reaches the focal region.[17] At the same time, the laser affected region is increasing,[17] similarly to the heat accumulation effects.[51,70] Solution of Maxwell's equations that are used in Ref. [17] requires enormous computer resources to be realized for multipulse irradiation regimes. Hence, a simplified but robust model could be useful for estimating the possible consequences of the defects accumulation.

The case of fused silica glass is considered here whose main defect states are well known. In fused silica, self-trapped excitons (trapped electron–hole pairs on broken Si–O bonds) are the primarily defects[72,73] with lifetime of ~400 ps at elevated temperatures.[74] App. 0.1% self-trapped excitons (STEs) are known to evolve into *E'*-centers which represent a silicon atom bonded to three oxygen atoms with one unpaired electron.[43] Other intrinsic defects in fused silica are NBOHCs (non-bridging oxygen hole centers, an oxygen atom bonded to one silicon atom with one unpaired electron) whose formation correlates well with radiation-induced densification.[75] Re-excitation of the laser-induced defects is an important route of free electron plasma generation at multi-pulse irradiation regimes as the energies of the defect states lie within the bandgap.[76] From pulse to pulse due to defect accumulation, the light absorption zone should extend toward the front sample surface from the focal region, thus enhancing attenuation of the beam in its way to the focus, though less effective as compared to pump-probe experiments with pico- and subpicosecond time separation between pulses.[17]

Following to Ref. [71] and further simplifying the model, a sequence of rectangular pulses is considered with the incident laser energy E_0. The laser beam intensity in (x,y,z) coordinates can be roughly expressed as

$$I(x,y,z)=\frac{E_0}{\pi^{2/3}w_0^2\tau_L\left(1+z^2/z_0^2\right)}\exp\left(-\frac{x^2+(y+vt)^2}{w_0^2\left(1+z^2/z_0^2\right)}\right). \tag{19}$$

Here z_0 is the Rayleigh length, z is the distance from the focal plane, w_0 is the beam waist, τ_L is the pulse duration, and v is the scanning velocity of the beam. For such pulses, disregarding collisional ionization, the free electron density generated by the end of the first pulse with wavelength of 800 nm can be evaluated via 6-photon ionization rate (see Sections 2-3) as

$$n_e^{(1)}=\sigma_6 I^6\tau_L\,. \tag{20}$$

$n_e^{(1)}$ is dependent on the intensity $I(x,y,z)$. Then, for the second laser pulse taking into account that only app. 0.1% of free electrons are converted to *E'*-centers whose ionization rate ionizable through the 4-photon ionization process (Section 3),[62,76] we can write:

$$n_e^{(2)}=\sigma_6 I^6\tau_L+10^{-3}\frac{n_e^{(1)}}{n_{at}}\sigma_4 I^4\tau_L \quad \text{or} \quad n_e^{(2)}=\sigma_6 I^6\tau_L+\frac{10^{-3}}{n_{at}}\sigma_6 I^6{\tau_L}^2\sigma_4 I^4\,. \tag{21}$$

Repeating this procedure for N pulses, one can write:

$$n_e^{(N)}=\sigma_6 I^6\tau_L+10^{-3}\frac{n_e^{(N-1)}}{n_{at}}\sigma_4 I^4\tau_L\,, \tag{22}$$

where $n_e(N\text{-}1)$ can be expressed via the accumulation of the defect states generated locally by the previous pulses. The laser intensity focusing with accounting for multiphoton ionization is calculated as[71]

$$\frac{\partial I}{\partial z}=-\frac{2zI}{z_0^2+z^2}-6\hbar\omega\sigma_6 I^6-10^{-3}\frac{n_e^{(N-1)}}{n_{at}}4\hbar\omega\sigma_4 I^4 \tag{23}$$

This equation allows to calculate the map of the absorbed laser energy

$$E_{abs}(x,y,z)=(I(x,y,z)-I(x,y,z-\Delta z))\Delta x\Delta y\tau_L \tag{24}$$

This term is introduced as a periodic energy source, depending on the pulse repetition rate, into the 3D heat diffusion equation which is solved similarly to Ref. [51]. The first results are presented in Fig. 7 where the temporal evolutions of maximum local temperature and the length of the structure (defined by reaching the annealing point) are shown. In these simulations, scanning velocity was taken to be 0. It is seen that at certain number of pulses the local temperature exceeds the glass melting point (~2000 K) which can lead to creation of bubbles in the molten material region as described in Section 2. However, with further irradiation the maximum temperature again drops to the values below the melting point, indicating that the irradiation regime can return to gentle modification of material. This observation can explain such an unusual effect as so-called phase transition, that is, a sudden change of modification in the laser track from melting or even bubble formation to gentle modification in the form of nanogratings, as observed in Ref. [31]. Under direct laser writing conditions with the beam scanning inside the glass, thousands of pulses may be required for proper formation of a shield sufficient to screen the laser beam to the level below the melting threshold that depends on the laser beam energy, pulse repetition rate, focusing conditions, and scanning speed. The presented model can give useful information on a qualitative trends of accumulation effects not only upon volumetric modification of materials but also for surface material processing. This study is now under the progress.

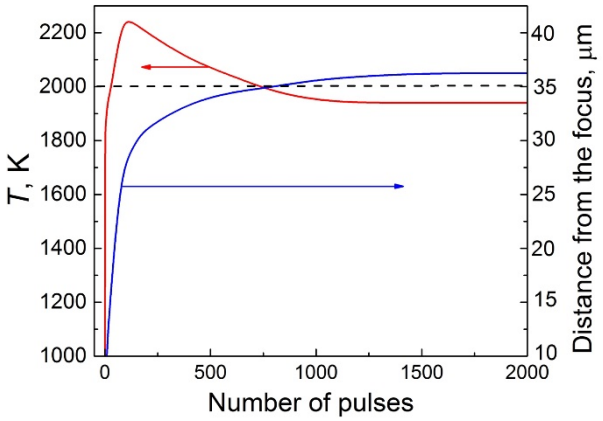

Figure 7. Maximum local temperature inside a fused silica sample, obtained by modeling of multipulse irradiation be a focused laser beam with accounting for the defect accumulation (red line). The length of the modification structure extending towards the irradiating laser from pulse to pulse (blue line).

5. CONCLUSIONS

In this paper, an overview of several models was presented which were developed to describe processes induced by ultrashort laser pulses inside and on the surface of bulk glass materials. The opto-thermoelastoplastic model allows for the detailed studies of spatiotemporal dynamics of the laser beam propagation through transparent optical materials and the evolution of the free electron plasma. Yielding the absorbed energy map, it further enables the thermoelastoplastic simulations of material redistribution. It has been revealed that the material modification occurs at very short time scales after the laser beam action, presumable at subnanosecond time when the laser induced stresses exceed the deformation/failure strength. To gain insight into the temperature evolution of a glass material upon irradiation its surface by ultrashort laser pulses, we employ a model based on the rate equation describing free electron generation coupled with the energy equations for electrons and lattice. Swift material heating to very high temperatures at fs timescale has been found at laser fluences exceeding the threshold fluence by 2-3 times. This can result in efficient bremsstrahlung emission from the irradiation spot as observed in experiments. The mechanisms of glass ablation with ultrashort laser pulses are discussed by comparing with experimental data. Finally, a new model is outlined for multi-pulse irradiation regimes which enables gaining insight into the roles of defects and heat accumulation.

ACKNOWLEDGEMENTS

This work was partially supported by several funding agencies. NMB, IM, and TM greatly acknowledge support of the state budget of the Czech Republic (project HiLASE: Superlasers for the

real world: LO1602). The study described in Section 2 was performed under a partial support of the Russian Foundation for Basic Research (Project No. 15-01-02432). The work of MPF related the model presented in Section 4 was suppoted by Russian Science Foundation (Project No. 14-21-00110). LF also acknowledges a financial support of the Prague Competitiveness Operational Programme (project FUNBIO, No. CZ.2.16/3.1.00/21568). *This work performed under the auspices of the U.S. Department of Energy by Lawrence Livermore National Laboratory under Contract DE-AC52-07NA27344.

REFERENCES

[1] Davis, K. M., Miura, K., Sugimoto, N., and Hirao, K., "Writing waveguides in glass with a femtosecond laser," Opt. Lett. 21, 1729-1731 (1996).
[2] Stuart, B. C., Feit, M. D., Rubenchik, A. M., Shore, B. W., and Perry, M. D., "Nanosecond to femtosecond laser induced breakdown in dielectrics", Phys. Rev.B. 53, 1749-1761 (1996).
[3] Glezer, E. N. and Mazur, E., "Ultrafast-laser driven micro-explosions in transparent materials," Appl. Phys. Lett. 71, 882-884 (1997).
[4] Homoelle, D., Wielandy, S., Gaeta, A. L., Borrelli, N. F., and Smith, C., "Infrared photosensitivity in silica glasses exposed to femtosecond laser pulses", Opt. Lett. 24, 1311-1313 (1999).
[5] Schaffer, C. B., Brodeur, A., Garca, J. F., and Mazur, E., "Micromachining bulk glass by use of femtosecond laser pulses with nanoJoule energy," Opt. Lett. 26, 93-95 (2001).
[6] Tzortzakis, S., Sudrie, L., Franko, M., Prade, B., Mysrowicz, A., Couairon, A., and Berge, L., "Self-focusing of few-cycle light pulses in dielectric media", Phys. Rev. Lett. 87, 213902 (2001).
[7] Streltsov, A. M. and Borrelli, N. M., "Study of femtosecond-laser-written waveguides in glasses," J. Opt. Soc. Am. B 19, 2496-2504 (2002).
[8] Will, M., Nolte, S., Chichkov, B. N., and Tünnermann, A., "Optical Properties of Waveguides Fabricated in Fused Silica by Femtosecond Laser Pulses," Appl. Opt. 41, 4360-4364 (2002).
[9] Osellame, R., Taccheo, S., Marangoni, M., Ramponi, R., Laporta, P., Polli, D., De Silvestri, S., and Cerlullo, G., "Femtosecond writing of active optical waveguides with astigmatically shaped beams", J. Opt. Soc. Am. B 20, 1559-1567 (2003).
[10] Florea, C. and Winick, K. A., "Fabrication and Characterization of Photonic Devices Directly Written in Glass Using Femtosecond Laser Pulses," J. Lightwave Technol. 21, 246-253 (2003).
[11] Gattass, R., and Mazur, E., "Femtosecond laser micromachining in transparent materials," Nature Photon. 2, 219-225 (2008).
[12] Mishchik, K., D'Amico, C., Velpula, P. K., Maclair, C., Boukenter, A., Ouerdane, Y., and Stoian, R. "Ultrafast laser induced electronic and structural modifications in bulk fused silica," J. Appl. Physics 114, 133502 (2013).
[13] Zimmermann, F., Plech, A., Richter, S., Tünnermann, A., and Nolte, S., "On the rewriting of ultrashort pulse-induced nanogratings," Opt. Lett. 40, 2049-2052 (2015).
[14] Derrien, T. J.-Y., Koter, R., Krüger, J., Höhm, S., Rosenfeld, A., and Bonse, J., "Plasmonic formation mechanism of periodic 100-nm-structures upon femtosecond laser irradiation of silicon in water," J. Appl. Phys. 116, 074902 (2014).
[15] Buividas, R., Mikutis M., and Juodkazis, S., "Surface and bulk structuring of materials by ripples with long and short laser pulses: Recent advances," Prog. Quantum Electron. 38(3), 119-156 (2014).
[16] Gamaly, E. G., Vailionis, A., Mizeikis, V., Yang, W., Rode, A. V., and Juodkazis, S., Warm dense matter at the bench top: Fs-laser-induced confined micro-explosion," High Energy Density Physics 8, 13-17 (2012).
[17] Bulgakova, N. M., Zhukov, V. P., Meshcheryakov, Y. P., Gemini, L., Brajer, J., Rostohar, D., and Mocek, T., "Pulsed laser modification of transparent dielectrics: What can be foreseen and predicted in numerical experiments," J. Opt. Soc. Am. B 31, C8-C14 (2014).
[18] Kazansky, P. G., Yang, W., Bricchi, E., Bovatsek, J., Arai, A., Shimotsuma, Y., Miura, K., and Hirao, K., ""Quill" writing with ultrashort light pulses in transparent materials," Appl. Phys. Lett. 90, 151120 (2007)
[19] Vitek, D. N., Block, E., Bellouard, Y., Adams, D. E., Backus, S., Kleinfeld, D., Durfee, C. G., and Squier, J. A., "Spatio-temporally focused femtosecond laser pulses for nonreciprocal writing in optically transparent materials," Opt. Express 18, 24673-24678 (2010).

[20] Gaeta, A. L., "Catastrophic collapse of ultrashort pulses," Phys. Rev. Lett. 84, 3582–3585 (2000).
[21] Couairon, A. and Mysyrowicz, A., "Femtosecond filamentation in transparent media," Phys. Rep. 441, 47–189 (2007).
[22] Burakov, I. M., Bulgakova, N. M., Stoian, R., Mermillod-Blondin, A., Audouard, E., and Rosenfeld, A., "Spatial distribution of refractive index variations induced in bulk fused silica by single ultrashort and short laser pulses," J. Appl. Phys. 101, 043506 (2007).
[23] Dostovalov, A.V., Wolf, A.A., Mezentsev, V.K., Okhrimchuk, A.G., amd Babin, S.A., "Quantitative characteriazation of energy absorption in femtosecond laser micro-modification of fused silica," Opt. Express 23, 32541-32547 (2015).
[24] Mézel, C., Hallo, L., Bourgeade, A., Hébert, D., Tikhonchuk, V. T., Chimier, B., Nkonga, B., Schurtz, G., and Travaillé, G., "Formation of nanocavities in dielectrics: A self-consistent modeling," Phys. Plasmas 15, 093504 (2008).
[25] Popov, K. I., McElcheran, C., Briggs, K., Mack, S., and Ramunno, L., "Morphology of femtosecond laser modification of bulk dielectrics, " Opt. Express 19, 271-282 (2010).
[26] Schmitz, H., and Mezentsev, V., "Full-vectorial modeling of femtosecond pulses for laser inscription of photonic structures," J. Opt. Soc. Am. B 29, 1208-1217 (2012).
[27] Bulgakova, N. M., Zhukov, V. P., and Meshcheryakov, Yu. P., "Theoretical treatments of ultrashort pulse laser processing of transparent materials: Towards understanding the volume nanograting formation and "quill" writing effect," Appl. Phys. B 113, 437-449 (2013).
[28] Bulgakova, N. M., Zhukov, V. P., Sonina, S. V., and Meshcheryakov, Yu. P., "Modification of transparent materials with ultrashort laser pulses: What is energetically and mechanically meaningful?" J. Appl. Phys. 118, 233108 (2015).
[29] Quéré, F., Guizard, S., and Martin, P. "Time-resolved study of laser-induced breakdown in dielectrics," Europhys. Lett. 56, 138 (2001).
[30] Temnov, V. V., Sokolowski-Tinten, K., Zhou, P., El-Khamhawy, A., and von der Linde, D., "Multiphoton ionization in dielectrics: Comparison of circular and linear polarization," Phys. Rev. Lett. 97, 237403 (2006).
[31] Puerto, D., Siegel, J., Gawelda, W., Galvan-Sosa, M., Ehrentraut, M., Bonse, J., and Solis, J., "Dynamics of plasma formation, relaxation, and topography modification induced by femtosecond laser pulses in crystalline and amorphous dielectrics," J. Opt. Soc. Am. B 27, 1065-1076 (2010).
[32] Du, D., Liu, X., Korn, G., Squier, J., and Mourou, G., "Laser-induced breakdown by impact ionization in SiO_2 with pulse widths from 7 ns to 150 fs," Appl. Phys. Lett. 64, 3071-3073 (1994).
[33] Lenzner, M., Krausz, J., Krüger, J., Kautek, W., "Photoablation with sub-10 fs laser pulses," Appl. Surf. Sci. 154-155, 11-16 (2000).
[34] Jiang, L., Tsai, H.-L., "A plasma model combined with an improved two-temperature equation for ultrafast laser ablation of dielectrics," J. Appl. Phys. 104, 093101 (2008).
[35] Chimier, B., Utéza, O., Sanner, N., Sentis, M., Itina, T., Lassonde, P., Légaré, F., Vidal, F., and Kieffer, J. C., "Damage and ablation thresholds of fused-silica in femtosecond regime," Phys. Rev. B 84, 094104 (2011).
[36] Hu, H., Wang, X., and Zhai, H., "High-fluence femtosecond laser ablation of silica glass: effects of laser-induced pressure," J. Phys. D: Appl. Phys. 44, 135202 (2011).
[37] Eaton, S. M., Zhang, H., Herman, P. R., Yoshino, F., Shah, L., Bovatsek, J., and Arai, A. Y., "Heat accumulation effects in femtosecond laser-written waveguides with variable repetition rate," Opt. Express, 13, 4708-4716 (2005).
[38] Miyamoto, I., Cvecek, K., Okamoto, Y., and Schmidt, "Internal modification of glass by ultrashort laser pulse and its application to microwelding," App. Phys. A 114, 187-208 (2014).
[39] Sun, M., Eppelt, U., Schulz, W., and Zhu., J., "Mechanism of internal modification in bulk borosilicate glass with picosecond laser pulses at high repetition rate," Proc. SPIE 9532, 953214 (2015).
[40] Caulier, O.D., Mishchik, K., Chimier, B., Skupin, S., Bourgeade, A., Leger, C. J., Kling, R., Honninger, C., Lopez, J., Tikhonchuk, V., and Duchateaux, G., "Femtosecond laser pulse train interaction with dielectric materials," Appl. Phys. Lett. 107, 181110 (2015).
[41] Peng, J., Grojo, D., Rayner, D. M., and Corkum, P. B., "Control of energy deposition in femtosecond laser dielectric interactions," Appl. Phys. Lett. 102, 161105 (2013).
[42] Grojo, D., Gertsvolf, M., Lei, S., Barillot, T., Rayner, D. M., and Corkum, "Exciton-seeded multiphoton ionization in bulk SiO_2," P. B., Phys. Rev. B 81, 212301 (2010).
[43] Petite, G., Guizard, S., Martin, P., and Quéré, F., "Comment on 'Ultrafast electron dynamics in femtosecond optical breakdown of dielectrics'," Phys. Rev. Lett. 83, 5182 (1999).
[44] Timoshenko, S. P., [Course of Theory of Elasticity], Naukova Dumka, Kiev, 1972 (in Russian).
[45] Meshcheryakov, Yu. P., Shugaev, M. V., Mattle, T., Lippert, T., and Bulgakova, N. M., "Role of thermal stresses on pulsed laser irradiation of thin films under conditions of mucrobump formation ond nonvaporization forward transfer," Appl. Phys. A 113, 521 (2013).

[46] Mermillod-Blondin, A., Mentzel, H., and Rosenfeld, A., "Time-resolved microscopy with random lasers," Opt. Lett. 38, 4112-4115 (2013).
[47] Bellouard, Y., and Hongler, M.-O., "Femtosecond-laser generation of self-organized bubble patterns in fused silica," Opt. Express, 19, 6807-6821 (2011).
[48] Hardy, S. C., "The motion of bubbles in a vertical temperature gradient," J. Colloid Interface Sci. 69, 157-162 (1979).
[49] Sakakura, M., Terazima, M., Shimotsuma, Y., Miura, K., and Hirao, K., "Thermal and shock induced modification inside a silica glass by focused femtosecond laser pulse," J. Appl. Phys. 109, 023503 (2011).
[50] Asada, T., Tamaki, T., Nakazumi, M., Ohmura, E., and Itoh, K., "Laser-induced structural modifications inside glass using a femtosecond laser and a CO_2 laser,"J. Laser Micro/Nanoeng. 9, 174-179 (2014).
[51] Shimizu, M., Sakakura, M., Ohnishi, M., Shimotsuma, Y., Nakaya, T., Miura, K., and Hirao, K., " Mechanism of heat-modification inside a glass after irradiation with high-repetition rate femtosecond laser pulses," J. Appl. Phys. 108, 073533 (2010).
[52] Yablonovitch, E., "Self-phase modulation and short-pulse generation from laser-breakdown plasmas," Phys. Rev. A 10, 1888-1895 (1974).
[53] Wood, Wm. M., Siders, C. W., and Downer, M. C., "Measurement of femtosecond ionization dynamics of atmospheric density gases by spectral blueshifting," Phys. Rev. Lett. 67, 3523-3526 (1991).
[54] Duchateau, G. and Bourgeade, A., "Influence of the time-dependent pulse spectrum on ionization and laser propagation in nonlinear optical materials," Phys. Rev. A 89, 053837 (2014).
[55] Ristau, D., [Laser-Induced Damage in Optical Materials], Boca Raton, Fla., CRC Press, Taylor & Francis Group, 2014.
[56] Haahr-Lillevang, L., Wædegaard, K., Sandkamm, D. B., Mouskeftaras, A., Guizard, S., Balling, P., "Short-pulse laser excitation of quartz: experiments and modelling of transient optical properties and ablation," Appl. Phys. A 120, 1221-1227 (2015).
[57] Schiffrin, A., Paasch-Colberg, T., Karpowicz, N., Apalkov, V., Gerster, S., Mühlbrandt, S., Korbman, M., Reichert, J., Schultze, M., Holzner, S., Barth, J. V., Kienberger, R., Ernstorfer, R., Yakovlev, V. S., Stockman, M. I., and Krausz, F., Nature 493, 70-74 (2013).
[58] Bulgakova, N. M., Stoian, R., Rosenfeld, A., Hertel, I. V., Marine, W., and Campbell, E. E. B., "A general continuum approach to describe fast electronic transport in pulsed laser irradiated materials: The problem of Coulomb explosion," Appl. Phys. A 81, 345-356 (2005).
[59] Bulgakova, N. M., Stoian, R, and Rosenfeld, A., "Laser-induced modification of transparent crystals and glasses," Quantum Electron. 40, 966-985 (2010).
[60] Burakov, I. M., Bulgakova, N. M., Stoian, R., Rosenfeld, A., and Hertel, I. V., "Theoretical investigations of material modification using temporally shaped femtosecond laser pulses," Appl. Phys. A 81, 1639-1645 (2005).
[61] Kaiser, A., Rethfeld, B., Vicanek, M., and Simon G. "Microscopic processes in dielectrics under irradiation by subpicosecond laser pulses," Phys. Rev. B, 61, 11437-11449 (2000).
[62] Martin, P., Guizard, S., Daguzan, Ph., Petite, G., D'Oliveira, P., Maynadier P., and Pedrix M., "Subpicosecond study of carrier trapping dynamics in wide-band-gap crystals," Phys. Rev. B 55, 5799-5810 (1997).
[63] Couairon, A., Sudrie, L., Franco, M., Prade, B., and Mysyrowicz, A., "Filamentation and damage in fused silica induced by tightly focused femtosecond laser pulses," Phys. Rev. B 71,125435 (2005).
[64] Geoffroy, G., Duchateau, G., Fedorov, N., Martin, P., and Guizard, S., "Influence of electron Coulomb explosion on photoelectron spectra of dielectrics irradiated by femtosecond laser pulses," Las. Phys. 24, 086101 (2014).
[65] Artsimovich, L. A. and Sagdeev, R.Z., [Plasma Physics for Physicists], Atomizdat, Moscow, 1979 (in Russian).
[66] Bulgakova, N. M., Evtushenko, A. B., Shukhov, Yu. G., Kudryashov, S. I., and Bulgakov, A. V., "Role of laser-induced plasma in ultradeep drilling of materials by nanosecond laser pulses," Appl. Surf. Sci. 257, 10876-10882 (2011).
[67] Karim, E. T., Wu, C., and Zhigilei, L. V., "Molecular dynamics simulations of laser-materials interactions: General and material-specific mechanisms of material removal and generation of crystal defects," Springer Series in Materials Science 195, 27-49 (2014).
[68] Bulgakova, N. M., Bulgakov, A. V., Zhukov, V. P., Marine, W., Vorobyev, V. Y., Guo, C., "Charging and plasma effects under ultrashort pulsed laser ablation," Proc. SPIE 7005, 70050C (2008).
[69] Bulgakova, N. M. and Bulgakov, A. V., "Comment on 'Time-Resolved Shadowgraphs of Material Ejection in Intense Femtosecond Laser Ablation of Aluminum'," Phys. Rev. Lett. 101, 099701 (2008).
[70] Sakakura, M., Shimizu, M., Shimotsuma, Y., Miura, K, and Hirao, K, "Temperature distribution and modification mechanism inside glass with heat accumulation during 250 kHz irradiation of femtosecond laser pulses," Appl. Phys. Lett. 93, 231112 (2008).

[71] Rayner, D. M., Naumov, A., and Corkum, P. B., "Ultrashort pulse non-linear optical absorption in transparent media," Opt. Express 13, 3208-3217 (2005).
[72] Itoh, N., Shimizu-Iwayama, T., and Fujita, T., "Excitons in crystalline and amorphous SiO_2: formation, relaxation and conversion to Frenkel pairs," J. Non-Cryst. Solids 179, 194-201 (1994).
[73] Guizard, S., Martin, P., D'Oliveira, P., and Maynadier, P., "Time-resolved study of laser-induced colour centres in SiO_2," J. Phys.: Condens. Matter 8, 1281-1290 (1996).
[74] Richter, S., Jia, F., Heinrich, M., Döring, S., Peschel, U., Tünnermann, A., and Nolte, S., "The role of self-trapped excitons and defects in the formation of nanogratings in fused silica," Opt. Lett., 37, 482-484 (2012).
[75] Schenker, R. E. and Oldham, W. G., "Ultraviolet-induced densification in fused silica," J. Appl. Phys. 82, 1065-1071 (1997).
[76] Vigouroux, J. P., Duraud, J. P., Le Moel, A., Le Gressus, C., and Griscom, D. L., "Electron trapping in amorphous SiO_2 studied by charge buildup under electron bombardment," J. Appl. Phys. 57, 5139-5144 (1985).
[77] Kazansky, P. G., Berezna, M., Gecevicius, M., Corbari, C., Shimotsuma, Y., Sakakura, M., Miura, K., Hirao, K., and Bellouard, Y., "Phase transition induced by ultrafast laser writing in transparent materials," in: [CLEO:2011—Laser Applications to Photonic Applications, OSA Technical Digest (CD)], Optical Society of America, paper JTuI106 (2011).